# Measuring the true hydroxide conductivity of anion exchange membranes

Avital Zhegur-Khais [a], Fabian Kubannek [b], Ulrike Krewer [d], Dario R. Dekel [a,c,*]

[a] The Wolfson Department of Chemical Engineering, Technion - Israel Institute of Technology, Haifa, 3200003, Israel
[b] TU Braunschweig, Institute of Energy and Process Systems Engineering, Franz-Liszt-Str. 35, 38106, Braunschweig, Germany
[c] The Nancy & Stephan Grand Technion Energy Program (GTEP), Technion - Israel Institute of Technology, Haifa, 3200003, Israel
[d] Karlsruhe Institute of Technology, Institute for Applied Materials (IAM-WET), Adenauerring 20b, 76131 Karlsruhe, Germany

ARTICLE INFO

*Keywords:*
Fuel cells
Anion exchange membrane
Hydroxide conductivity
Hydroxide diffusivity
Decarbonation

ABSTRACT

In this study, a $CO_2$-in-situ purging technique was used to measure the true $OH^-$ conductivity of several anion exchange membranes (AEMs). During this process, membranes are in-situ de-carbonated allowing the AEMs to reach their full $OH^-$ form, and therefore to measure their highest (true) $OH^-$ conductivity. The de-carbonation process in all the studied AEMs was also investigated. The time constant of the de-carbonation process $\tau$ was calculated and related to the membrane properties as well as to the de-carbonation dynamics. The time constant of the de-carbonation process was found to decrease with increasing current densities and decreasing the IEC of the membranes. This work provides unique and important data crucial to increasing the understanding of the main factors that may mitigate the de-carbonation process in AEMs to allow AEM fuel cells to be operated with ambient air.

## 1. Introduction

Anion-exchange membrane fuel cells (AEMFCs) have recently gained increased attention as the alkaline environment of the solid polyelectrolyte enables the use of low-cost materials, offering then a low-cost solution for fuel cells [1–5]. Over the last decade, there was a continuous improvement in the $H_2$-based AEMFCs performance [6–8], currently reaching power densities over 3 W $cm^{-2}$ at relatively high voltages [9]. Having high performance is essential for AEMFC to be feasible in practical applications; however, there are still a few challenges to be overcome – among them, there is a need of increasing the chemical stability of the anion exchange membranes (AEMs) [10–16], increasing the activity of electrocatalysts towards the hydrogen oxidation reaction [17–20], and decreasing the negative effect of $CO_2$ on the AEMs. Although the first two challenges are largely studied, the latter is scarcely investigated. Despite its importance, the effect of $CO_2$ on the AEMs is not yet well studied. Most fuel cell tests are done under pure oxygen (or $CO_2$-filtered or $CO_2$-free air) without taking into consideration the effect of $CO_2$ on fuel cell operation [21]. Just a very few studies were devoted to investigate the effect of $CO_2$ on the AEMs [22–24], and almost no work was done on the dynamics of the carbonation and de-carbonation process of the AEMs [22,25–27].

When ambient air is used as a source of oxidant to operate an AEMFC, the hydroxide generated from the oxygen reduction reaction on the cathode side quickly reacts to produce (bi)carbonate anions (Eqs. (1) and (2)). There is still a debate over which ion is dominant in the AEM after introducing ambient $CO_2$, bicarbonate [25,28] or carbonate [29]. Nevertheless, it is agreed that both anions are much bulkier and have lower mobility (related to the larger ionic radius and mass of these anions [30,31]) than the hydroxide anion. Their lower mobility dramatically limits the ionic conductivity in the membrane and the ionomer in the catalyst layers, which reduces the overall fuel cell performance by around half [32,33].

$$OH^- + CO_2 \leftrightarrow HCO_3^- \quad (1)$$

$$HCO_3^- + OH^- \leftrightarrow CO_3^{2-} + H_2O \quad (2)$$

While introducing ambient $CO_2$, the equilibrium reactions of the carbonation process (Eqs. (1) and (2)) tend to be in favor of the formation of bicarbonate and carbonate species rather than hydroxide, causing an almost complete conversion in the matter of up to several hours, although most of the carbonation happens within the first minutes [34–37]. This caused difficulties in measuring the $OH^-$ conductivity as the membrane should be held at any time of the measurement in a $CO_2$-free environment. That requires the use of a glovebox, which complicates the measurement procedure as well.

* Corresponding author. The Wolfson Department of Chemical Engineering, Technion - Israel Institute of Technology, Haifa, 3200003, Israel.
*E-mail address:* dario@technion.ac.il (D.R. Dekel).

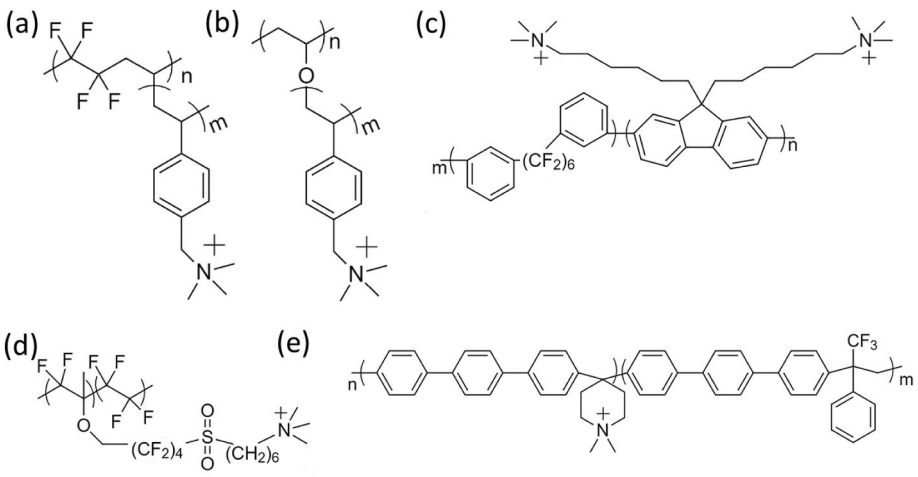


**Scheme 1.** General chemical structures of the research AEM studied in this work. (a) ETFE-TMA, (b) LDPE-BTMA, (c) QPAF-4(TM), (d) PF-AEM and (e) PAPip.

Measurements of $CO_3^{2-}$ and $HCO_3^-$ conductivity of AEMs in the literature mostly range between 2.2 and 5.4 times lower than the values measured for $OH^-$ conductivity [21,38]. Reduction in anion conductivity also occurs due to the lower degree of dissociation of carbonate anions from the membrane functional groups (FGs) [39–41], which means that fewer anions are free to move through the membrane. Also, $OH^-$ anions are transported through the Grotthuss (proton hopping) mechanism, as opposed to $CO_3^{2-}$ and $HCO_3^-$, which rely on diffusion, convection, and migration alone [42,43]. While $CO_3^{2-}$ and $HCO_3^-$ have a detrimental effect on the membrane conductivity, it was found that they can increase the AEM chemical stability compared to the case of $OH^-$, as (bi)carbonate anions are weaker nucleophiles than hydroxide anion [44]. This increase in stability was recently confirmed by a molecular dynamics study, which shows that carbonate ions are strongly coordinated to the quaternary ammonium (QA) (of the AEMs), reducing then the hydroxide ions access to the QA, therefore stabilizing the AEM [45]. However, the same study showed that the presence of carbonate anions reduces the water solvation of the hydroxides, making them significantly more reactive towards the QA, reducing then the stability of the AEMs [45].

To reduce the negative effect of the (bi)carbonate anions in the system, it was found that when AEMFCs are operated at higher current densities, the $CO_3^{2-}$ and $HCO_3^-$ concentration could decrease significantly due to the $CO_2$ purging mechanism [35,46,47]. Carbonate is being pushed out from the cell as a result of the high rate of hydroxide production on the cathode, which exceeds the $CO_2$ absorption rate from the ambient air. Recently, based on the $CO_2$ purging mechanism, a method was developed to measure the true $OH^-$ conductivity of AEMs [26]. By applying direct current and inducing water splitting in the membrane, $OH^-$ is produced inside the AEM. The generated $OH^-$ anions purge the bicarbonate species out in the form of $CO_2$, enabling to in-situ exchange the AEM to its fully $OH^-$ form. This new technique to measure what was called the true $OH^-$ of AEMs has been adopted in studies recently carried out by Holdcroft et al. [27] and Varcoe et al. [48]. The concept and procedure to measure the true $OH^-$ were very recently expanded by Dekel et al. to ex-situ measure the chemical stability of AEMs in presence hydroxide anions [49].

We use this new technique to measure the true $OH^-$ conductivity and to study the de-carbonation ($CO_2$ purging) dynamics of different AEMs. Studying the transient change in anion conductivity during the de-carbonation process in AEMs is critical for the operation of AEMFCs under ambient conditions. Understanding the parameters that impact the de-carbonation process and its dynamics will help to develop improved AEMs for advanced AEMFCs that can be efficiently operated with ambient air (containing $CO_2$). In this study we analyze the purging mechanism process on a variety of different available AEMs, aiming to increase the understanding of the de-carbonation process in AEMs. Results may significantly contribute to the knowledge and understanding of AEM behavior during the operation of AEMFCs under ambient air.

## 2. Experimental

### 2.1. Anion exchange membranes

Both commercially available, as well as AEMs obtained from different research groups, were used in this study. The AEMs investigated includes Tokuyama A201 (Tokuyama Corporation, Japan); Sustainion® RT and Sustainion® Grade 60 (Dioxide Materials, USA), named hereafter Sustainion RT and Sustainion 60, respectively; AT-1 (Hespas-Energy, China); FAA-3 (FuMaTech, Germany); ETFE-TMA (ethylene tetrafluoroethylene functionalized with trimethylamine) and LDPE-BTMA (low-density polyethylene functionalized with benzyl trimethylamine) [50,51] developed and supplied by Prof. Varcoe (Surrey University, UK); PF-AEM (perfluorinated anion exchange membrane) [52] obtained from Dr. Pivovar (National Renewable Energy Laboratory, CO, USA), named hereafter PF; PAPip (polybiphenyl N-methyl piperidine) membrane [53] obtained from Prof. Jannasch (Lund University, Sweeden); and QPAF-4(TM) (perfluoroalkylene and fluorine-based copolymer functionalized with hexyl trimethyl ammonium) [54] obtained from Prof. Miyatake (Yamanashi University). The available chemical structures of the (non-commercial) AEMs are seen in Scheme 1. Prior to the conductivity measurement, all the membranes were exchanged to their bicarbonate form at room temperature, by immersing the AEM into a 1 M $KHCO_3$ aqueous solution for 48 h (solution exchanged three times per 24 h) and then thoroughly washed in milli-Q water (18.2 MΩ) for 48 h (water exchanged three times per 24 h), to remove the remaining $KHCO_3$.

### 2.2. Ion exchange capacity (IEC)

IEC of all AEMs was measured using the procedure previously reported [55]. In brief, the exchange from one ionic form into the other was done by soaking the membranes in 1 M KX (X  $Cl^-$, $NO_3^-$) for 48 h to exchange to $X^-$. First, all membranes were exchanged to $Cl^-$ then washed in milli-Q water for 48 h. The $Cl^-$ is then taken out of the membrane by exchanging into $NO_3^-$ form. Then the $KNO_3$ solution in which the membranes were soaked in is titrated with 0.01 M $AgNO_3$. After soaking the membrane in 1 M $KNO_3$ the membrane was washed in milli-Q water as mentioned before and dried overnight in a vacuum oven to obtain the dry weight. The IEC is finally calculated as shown elsewhere [55].

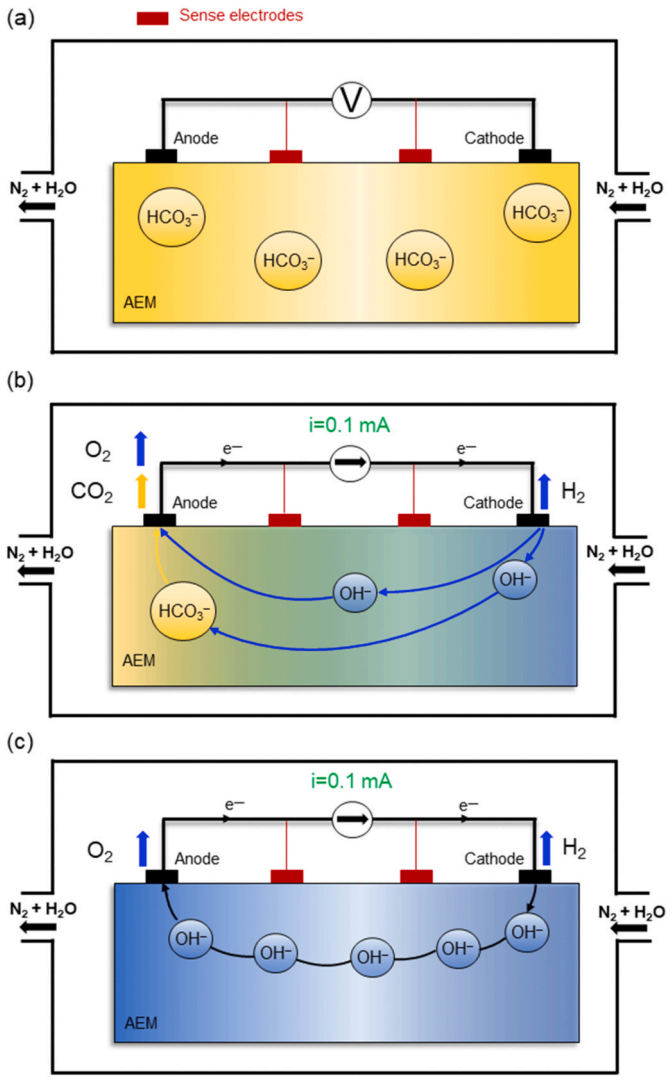


**Scheme 2.** Schematic illustration of the experimental setting of the de-carbonation process and the measurement of the true $OH^-$ conductivity. (a) The initial stage; measurement of the $HCO_3^-$ conductivity; (b) applying 0.1 mA direct current, forming $OH^-$ ions and purging the $HCO_3^-$ at the anode in the form of $CO_2$; and (c) true $OH^-$ conductivity achieved when the membrane is fully exchanged to $OH^-$.

### 2.3. Water uptake (WU)

WU of the AEMs in their $HCO_3^-$ form was measured using the procedure previously reported elsewhere [55], at the same temperature and humidity values as done in the de-carbonation tests (40 °C and 95% RH). In brief, the AEMs were first dried in-situ at 60 °C (~0% RH) to obtain the dry weight. Afterward, the conditions were changed to 40 °C and 95% RH and remained there until stabilization of the weight was achieved (<0.001 wt% change in 5 min).

### 2.4. True $OH^-$ conductivity

To measure the true $OH^-$ conductivity of the AEMs, the protocol recently described in Ziv and Dekel's work was used [26]. In brief, the AEM in its bicarbonate form was located into a four-probe electrode (MTS 740, Scribner Associates Inc.) for measuring the anion conductivity (see Scheme 2). The $HCO_3^-$ conductivity was measured for *ca.* three hours to ensure the stabilization of the membrane in the temperature and humidity atmosphere. Through the external electrodes, a constant direct current of 0.1 mA was applied to the membrane under

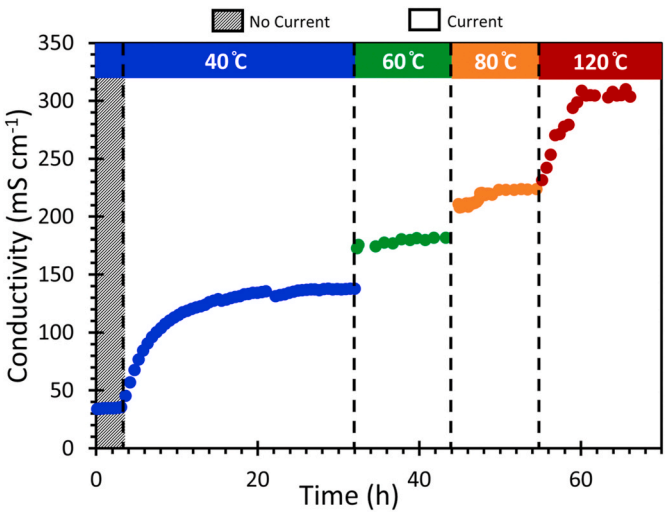


**Fig. 1.** Changes in the anion conductivity during the de-carbonation ($CO_2$ purging) process in-situ an AEM. The test is done on LDPE-BTMA AEM, at 0.1 mA direct current, under nitrogen flow at 95% relative humidity. The true $OH^-$ conductivity is measured at 40, 60, 80, and 120 °C.

nitrogen flow at 40 °C and relative humidity (RH) of 95%. The anion conductivity was continuously measured until conductivity reached a stable value (<0.1 kΩ change in resistance of 3 h). This conductivity value is called the true $OH^-$ conductivity [26]. After reaching the true $OH^-$ conductivity value at 40 °C, the temperature was rapidly increased to 60 °C (in the case of LDPE-BTMA even to 80 and 120 °C) at the same RH. The $OH^-$ conductivity was also continuously monitored during this time. All the conductivity measurements were done at ambient pressure, except for those measured at 120 °C, where a constant pressure of 200 kPa was used.

For each membrane, the time constant τ was calculated for the de-carbonation process from $HCO_3^-$ to $OH^-$ by fitting the conductivity data to an exponential equation [55,56],

$$\sigma^t \quad \sigma_0 + d\sigma\left(1 \quad \exp\left(\quad \frac{t}{\tau}\right)\right) \tag{3}$$

where $\sigma^t$ is the anion conductivity at time t, $\sigma_0$ is the initial conductivity (in $HCO_3^-$ form), and dσ is the difference between the final and the initial conductivity.

### 2.5. Diffusivity coefficients

Diffusivity coefficients for hydroxide and carbonate were calculated for each membrane using the Nernst-Einstein relation

$$D^i \quad \frac{\sigma RT}{cF^2z^2} \tag{4}$$

where $D^i$ is the diffusivity coefficient of species i, σ the conductivity, R the universal gas constant, $T$ the temperature, $c$ the concentration of the anion, F the Faraday constant, and $z$ the charge number of the ion.

The anion concentrations for Eq (4) were calculated by relating the number of anions to the entire membrane volume. Other approaches consider only the volume of liquid water in the membrane, which leads to higher concentration values because the same amount of ions is present in only a fraction of the membrane volume [57]. We decided to calculate the concentrations based on the entire membrane volume as this simple approach allows us to get a rough estimation of the diffusivities based on the available (measured) conductivity data.

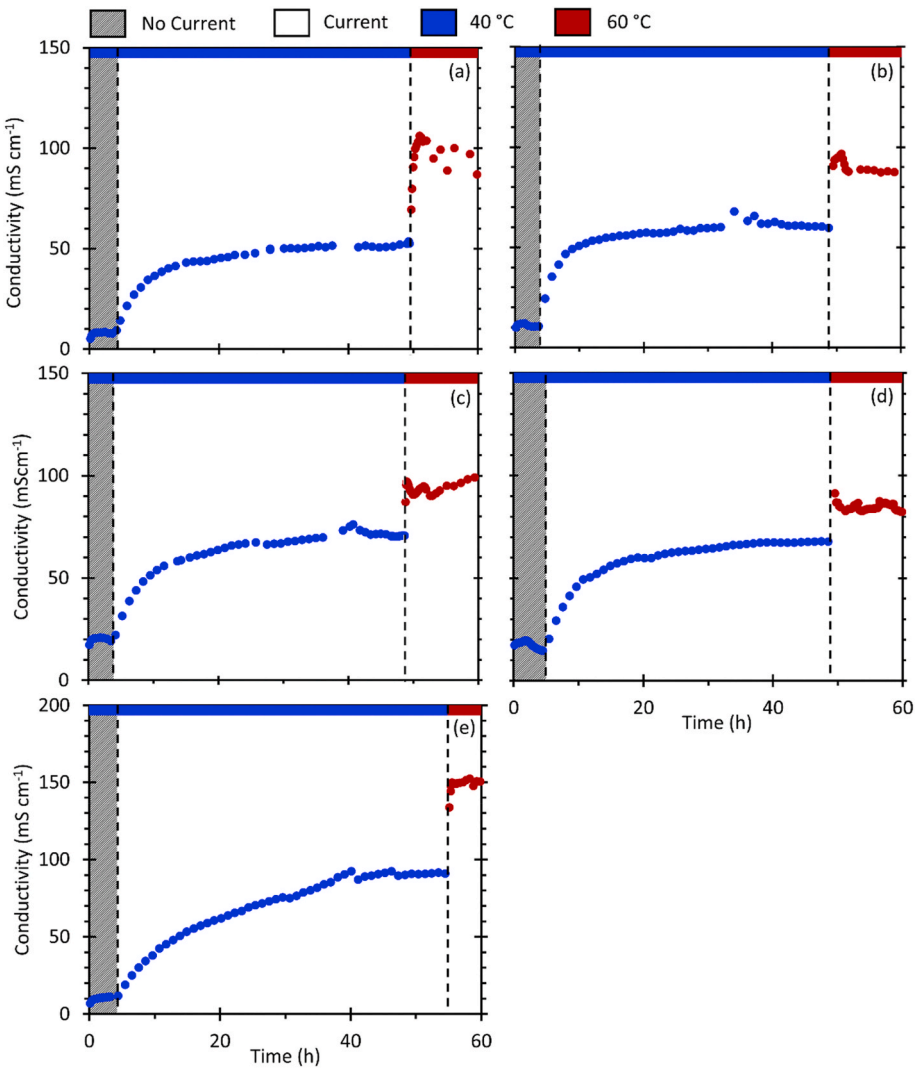


**Fig. 2.** Changes in commercial AEMs anion conductivity before and after applying 0.1 mA direct current. Conductivity was measured at 95% RH and 40 °C. After reaching the full $OH^-$ form, the temperature was increased to 60 °C (at 95% RH) and the conductivity was continuously measured for (a) FAA-3, (b) A201, (c) Sustainion 60, (d) Sustainion RT, and (e) AT-1 AEMs.

## 3. Results and discussion

The true $OH^-$ conductivity was measured by using the technique established by Ziv and Dekel [26] but applying different temperatures. Fig. 1 shows the anion conductivity values of the LDPE-BTMA AEM during the de-carbonation process over time. During the first hours (<5 h), the membrane stabilizes with the temperature (40 °C) and humidity (95% RH). The $HCO_3^-$ conductivity is determined as the average value of the conductivity after it reached a steady value. Afterward, a direct current of 0.1 mA is applied, triggering water electrolysis onto the membrane surface, producing $OH^-$ ions. This process causes the anion conductivity to rise gradually, as it can be seen by the exponential-like curve in blue (Fig. 1). The $OH^-$ ions migrate through the AEM to the anode electrode (see Scheme 2) purging the (bi)carbonate ions out of the membrane in the form of $CO_2$ (Eq. (1)) [26].

As can be seen in Fig. 1, during the de-carbonation test, the anion conductivity of the AEM is increased, as a result of the exchange of the $HCO_3^-$ anions to the $OH^-$ anions. When all the anions are exchanged and the AEM reaches its fully $OH^-$ form, the conductivity reaches its maximum value, which is called the true $OH^-$ conductivity [26] of the AEM. After the true $OH^-$ conductivity value was reached, the temperature was increased (while keeping 95% RH constant) and the true $OH^-$ conductivity of the LDPE-BTMA AEM was also measured at 60, 80, and 120 °C (Fig. 1). The rapid increase in conductivity from 40 to 60 °C and 60–80 °C further confirms that the AEM was in its full $OH^-$ form.

The $HCO_3^-$ conductivity of the LDPE-BTMA measured at 40 °C was 34 mS $cm^{-1}$. The true $OH^-$ conductivities measured at 40, 60, and 80 °C were 137 mS $cm^{-1}$, 180 mS $cm^{-1}$, and 223 mS $cm^{-1}$, respectively. These $OH^-$ conductivity values are higher than those reported in the literature – 102 and 126 mS $cm^{-1}$ [58] measured at 40 and 60 °C, respectively, as the true $OH^-$ conductivity in-situ procedure assures to achieve the fully $OH^-$ form of the AEM, with no $CO_2$ contamination. The true $OH^-$ conductivity of the LDPE-BTMA membrane was also measured at 120 °C, reaching an impressive value of 304 mS $cm^{-1}$, which to the best of our knowledge, is significantly higher than any other conductivity value measured up to date in AEMs. This extremely high conductivity value is achieved not only due to the high temperature of the measurement (until now, to the best of our knowledge, the highest temperature for conductivity measurement in AEMs was 100 °C [59,60]) but mainly because the measurement of the true $OH^-$ assures the AEM is in its full $OH^-$ form, providing then higher (and correct) $OH^-$ conductivity values.

Following the same procedure, we have measured the true $OH^-$ conductivity values of different AEMs, focusing on measurement at 40 and 60 °C. Fig. 2 and Fig. 3 show the conductivity values measured during the de-carbonation process for both commercial and research AEMs. The LDPE-BTMA membrane shows the highest conductivity

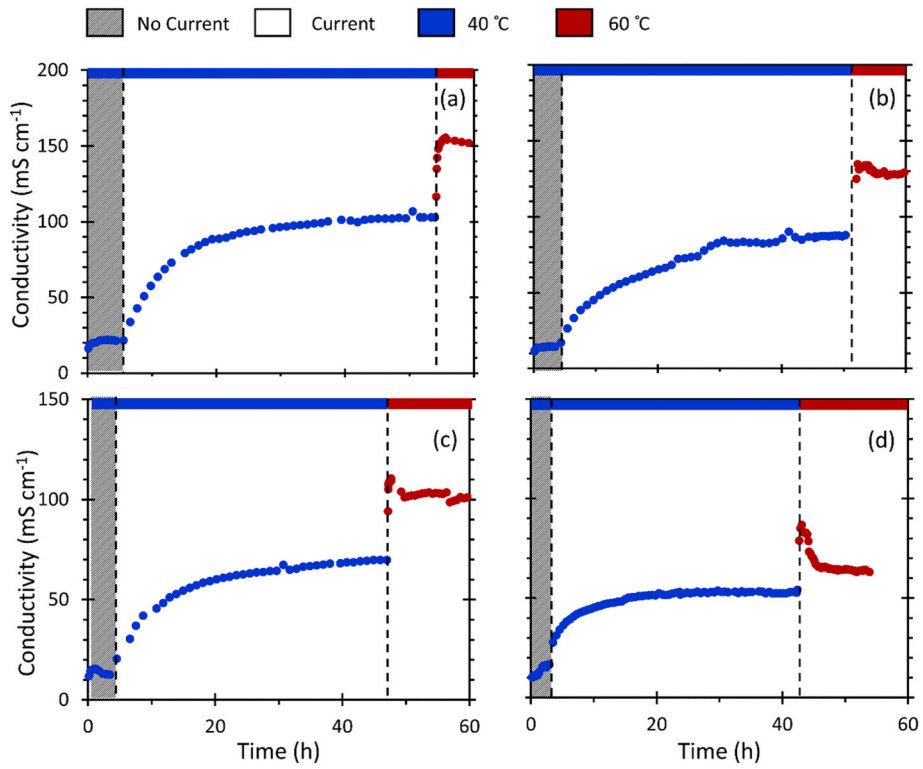


**Fig. 3.** Changes in research AEMs anion conductivity before and after applying 0.1 mA direct current. Conductivity was measured at 95% RH and 40 °C. After reaching the full $OH^-$ form, the temperature was increased to 60 °C (at 95% RH) and the conductivity was continuously measured for (a) ETFE-TMA, (b) PAPip, (c) PF, and (d) QPAF-4(TM) AEMs.

**Table 1**
Measured properties of the AEMs.

| | This work | | | | | | Literature values | | |
|---|---|---|---|---|---|---|---|---|---|
| | IEC (mmol $g^{-1}$) | WU (%) | $\sigma^{HCO3^-}$ (mS $cm^{-1}$) | $\sigma^{OH^-}$ (mS $cm^{-1}$) | | $\sigma OH^-/\sigma^{HCO3^-}$ | [a]$\sigma^{OH^-}$ (mS $cm^{-1}$) | | |
| | | | 40 °C | 40 °C | 60 °C | 40 °C | 40 °C | 60 °C | Ref. |
| **A201** | 1.58 | 38.2 | 10 | 60 | 88 | 6.0 | 36 | 48 | [67] |
| **FAA-3** | 1.43 | 26.2 | 8 | 51 | 101 | 6.4 | 22 | 35 | [68] |
| **Sustanion 60** | 1.44 | 50.6 | 20 | 70 | 97 | 3.5 | N/A | N/A | [69] |
| **Sustanion RT** | 1.47 | 52.3 | 15 | 67 | 82 | 4.5 | N/A | N/A | [69] |
| **AT-1** | 2.12 | 30.4 | 11 | 91 | 146 | 8.3 | 49[c] | 137[d] | [70] |
| **ETFE-TMA** | 1.59 | 43.5 | 21 | 102 | 152 | 4.9 | 60 | 112 | [25] |
| **LDPE-BTMA** | 2.39 | 74.8 | 34 | 137 | 180 | 4.2 | 102 | 126 | [58] |
| **PAPip** | 1.85 | 37.4 | 14 | 87 | 130 | 6.2 | 73 | 97 | [53] |
| **PF** | 0.92 | 25.9 | 13 | 70 | 102 | 5.4 | 57 | 85 | [71] |
| **QPAF-4(TM)** | 1.07 | 26.4 | 13 | 53 | 64 | 4.1 | 53 | 67 | [54] |

[a] Hydroxide conductivity values from the literature, measured at 40 °C and 60 °C, using liquid electrolyte soaking standard method - soaking the AEM in KOH (or NaOH) aqueous solution with posterior extensive water washing to remove the excess KOH.
[c] Conductivity measured at 30 °C.
[d] Conductivity measured at 80 °C.

values. Other AEMs such as ETFE-TMA, AT-1, PAPip, PF-AEM, and FAA-3, were also found to be highly conducting, reaching true $OH^-$ conductivity values (measured at 60 °C) higher than 100 mS $cm^{-1}$ (see Fig. 3). While similar high conductivity values (>100 mS $cm^{-1}$) were recently reported in the literature for other AEMs, those measurements were obtained at higher temperatures (≥70 °C) and not at 60 °C as done in this work [61–66]. For most of the AEMs, the $OH^-$ conductivity values measured using this liquid electrolyte-free technique were higher than the conductivity values reported in the literature, which were based on the current standard techniques the AEMs. Again, this is because this conductivity measurement method assures that the AEM is in its fully $OH^-$ form, therefore showing its highest $OH^-$ conductivity. A comparison between conductivity values measured in this study and those previously reported in the literature are summarized in Table 1. The AEMs were characterized by their IEC and WU, as previously described in the experimental section. The results are also summarized in Table 1. For the studied AEMs, the IEC measured ranges from 0.92 up to 2.39 mmol $g^{-1}$ and the WU values are in the 25.9–74.8% range (see Table 1).

For each AEM, the conductivity values measured during the de-carbonation process can be fitted to an exponential equation (Eq. (3)), from which τ, the time constant can be extracted. The parameter τ represents the dynamics of the de-carbonation process of the AEM. The calculated τ value for each membrane is shown in Table 2. As can be

**Table 2**
The calculated time constants τ and diffusivity coefficients of the different AEMs at 40 °C.

| | τ (h) | Cross-section Area $(cm^2)*10^{3}$ | [a]$D^{HCO3^-}$ $(m^2 s^{-1})$ $*10^{10}$ | [a]$D^{OH^-}$ $(m^2 s^{-1})$ $*10^{9}$ |
|---|---|---|---|---|
| **A201** | 3.6 | 3.3 | 1.9 | 1.1 |
| **FAA-3** | 6.2 | 2.5 | 1.6 | 1.0 |
| **Sustainion 60** | 7.6 | 9.7 | 3.9 | 1.9 |
| **Sustainion RT** | 7.0 | 10 | 3.2 | 1.7 |
| **AT-1** | 14.1 | 7.4 | 1.4 | 1.2 |
| **ETFE-TMA** | 8.1 | 4.2 | 3.4 | 1.6 |
| **LDPE-BTMA** | 8.2 | 6.5 | 4.4 | 1.8 |
| **PAPip** | 12.5 | 6.7 | 2.1 | 1.3 |
| **PF-AEM** | 9.1 | 5.4 | 3.7 | 2.0 |
| **QPAF-4(TM)** | 3.8 | 2.8 | 3.4 | 1.4 |

[a] Ion diffusivity values calculated from Eq. (4) conductivity are taken as the stabilized value from Figs. 2 and 3.

seen, A201 and QPAF-4(TM) membranes exhibited the shortest de-carbonation time constant τ of 3.6 and 3.8 h, respectively, meaning the de-carbonation process in these AEMs is the fastest as compared to other membranes. Interestingly, it is easy to assume that if an AEM exhibits both high $OH^-$ and $HCO_3^-$ conductivities, the de-carbonation will occur faster, since the mobility of the ions involved in the process is faster. However, this is not the case with A201 and QPAF-4(TM). Although they have moderate conductivities, the de-carbonation process is the fastest.

The rate at which each membrane is being exchanged from $HCO_3^-$ to $OH^-$ form is determined by, additionally to the current density, the rates at which these anions transport from the cathode to the anode electrodes. One of the main factors to influence this rate is dictated by the diffusivity of the anions. The diffusivity coefficient values of $HCO_3^-$ and $OH^-$ were estimated (Eq. (4)) and summarized in Table 2. The ratio between $OH^-$ and $HCO_3^-$ conductivities obtained by utilizing the true $OH^-$ conductivity was higher than what was frequently observed in the literature. In this work we found that the $OH^-/CO_3^{2-}$ conductivity ratio is in the range of 4.1–8.3, as compared to what was mainly reported in the literature, 2.2–5.0 [21]. We believe that this range represents the correct ratio, as in this study we use the true $OH^-$ conductivities, which are higher than those reported before.

For all the AEMs, diffusivity coefficients of $OH^-$ ions were found to be from three up to six times higher than those of $HCO_3^-$ ions, consistent with the literature values reported, which are in the same range [39,57]. While the calculated diffusion coefficients are within the range of literature values from Refs. [72–77], they are higher than those reported for proton exchange membranes [78]. This is surprising considering the higher diffusion coefficient of protons compared to hydroxide ions in water. The reason might be the fact that the Nernst-Einstein relation, which we used here, is not always applicable in AEM since the mechanisms of hydroxide transport depend on the membrane hydration [23]. Thus, the values can be used to compare our data with each other and with diffusivities from literature based on the Nernst-Einstein relation. The estimated $HCO_3^-$ and $OH^-$ diffusivities are in the range of 1.4–3.4 × $10^{-10}$ and 1.0–2.0 × $10^{-9}$ $m^2 s^{-1}$, respectively. They are consistent with those reported in the literature, even though there could be some differences since the measured $OH^-$ conductivities are higher in this study [72,79–81]. For instance, Marino et al. measured the FAA-3 $OH^-$ conductivity and calculated the diffusivity coefficient at room temperature at different water content. Diffusivity coefficient was ranging from 7.0 × $10^{-11}$-2.1 × $10^{-9}$ $m^2$ $s^{-1}$ for the water content of 65 down to 6, respectively [73]. Zelovich et al. [72,75] conducted ab-initio molecular dynamics studies of the AEM $OH^-$ diffusivity coefficient, the simulated values were found to be ranging from 1.8 × $10^{-10}$-4.2 × $10^{-9}$. Zadok et al. [74] performed molecular dynamics studies to obtain the $OH^-$ diffusivity coefficient for the PPP-BTEA polymer segment. The $OH^-$ diffusivity coefficient was ranging at about 7 × $10^{-10}$-7x$10^{-8}$ $m^2$ $s^{-1}$,

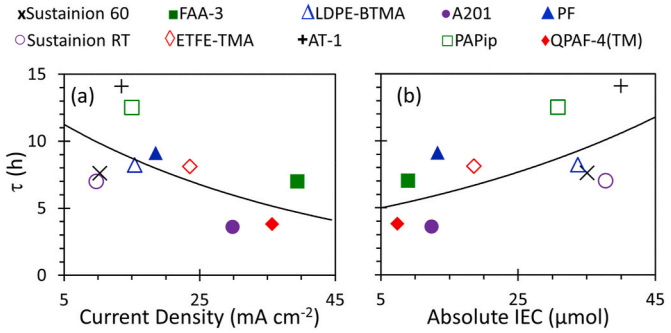


**Fig. 4.** The time constant τ as a function of (a) current density applied for each AEM and (b) the absolute IEC (calculated from the concentration of the FGs and the membrane volume).

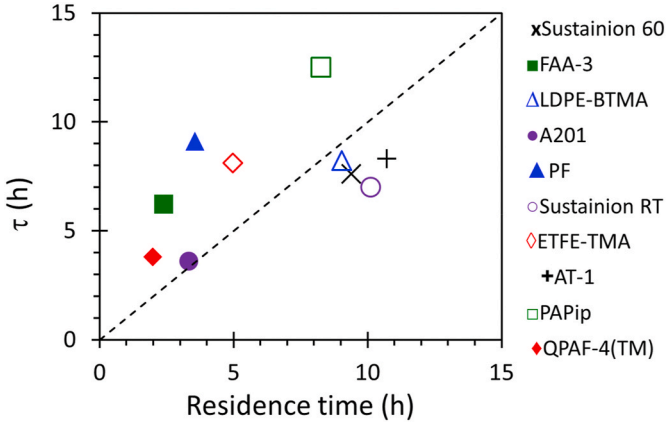


**Fig. 5.** The time constant τ as a function of residence time calculated for each AEM corresponded to the IEC.

which were obtained for a wide range of water content, up to 400.

To analyze the potential relationship between the different parameters (calculated and measured) and their effect on the de-carbonation process in the AEMs, the time constant τ was plotted against other AEM parameters. As seen in Fig. 4, τ is strongly affected by the IEC of the AEMs. A similar phenomenon was observed in a recent study, where a series of PPO-TEA AEMs, τ increased with IEC [82]. Also, τ it significantly decreases with a rise in current density (defined as the current applied at the conductivity measurement divided by the cross-sectional area of the AEM, which can be found in Table 2). Higher current density means higher production of $OH^-$ ions, therefore a higher $OH^-$ flux to the anode. This will purge the carbonates faster from the AEM. Lower IEC means that fewer carbonates need to be replaced by $OH^-$, which also reduces the de-carbonation time.

Both contributions, of the IEC and current, could be combined into a single parameter showing their effect simultaneously. With IEC and current, the residence time for each AEM could be calculated by nF/I, where n is the number of FGs present in an AEM in μmol, I is the current applied on the AEM (100 μA), and F is the Faraday constant. Residence time represents the time it takes for the AEM to produce the amount of $OH^-$ to replace all the $HCO_3^-$ ions. As seen in Fig. 5, τ is following a linear trend with the residence time, meaning that the de-carbonation process is indeed happening as a simple exchange of ions.

To try to get further information about the de-carbonation process τ was plotted against the ion diffusivity coefficients. The results are shown in Fig. 6 a and b. The time constant τ is seen not to have a distinct trend with $OH^-$ and $HCO_3^-$ diffusivities, opposite to what would be expected. The $HCO_3^-$ diffusivities have a slightly decreasing trend with τ, meaning as the diffusion coefficient increases the de-carbonation time lowers. In

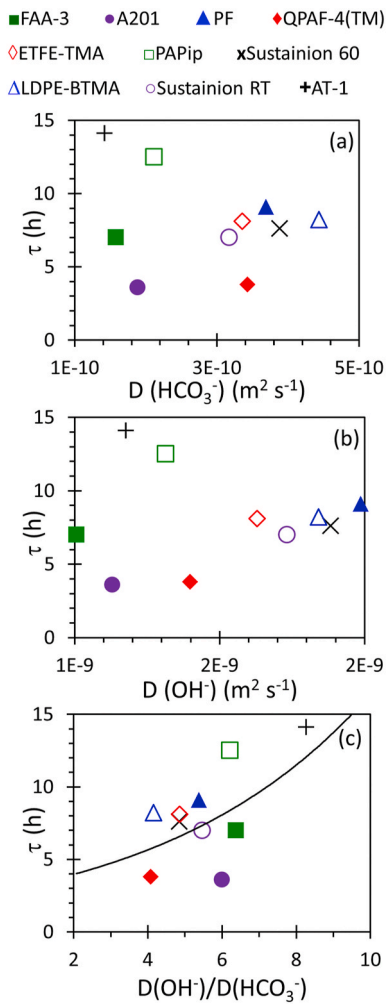


**Fig. 6.** The time constant τ of the de-carbonation process as a function of (a) $OH^-$ diffusivity coefficients, (b) $HCO_3^-$ diffusivity coefficients, (c) ratio between $OH^-/HCO_3^-$ diffusivities.

the case of $OH^-$ diffusivity, τ decreases and then increases again. It seems that the ratio of the hydroxide and carbonate diffusion coefficients rather than their absolute values governs the de-carbonation time. In Fig. 6c it can be seen that the de-carbonation time increases with the ratio $D^{OH^-}/D^{HCO3^-}$. The relative contribution of an anion to the total ionic current in the membrane increases with its ion mobility since all ions are driven by the same potential gradient. When hydroxide mobility is large compared to bicarbonate mobility, the de-carbonation process thus takes more time because the external current is mainly sustained by hydroxide transport whereas bicarbonate moves slowly.

## 4. Conclusions

In this work, we use our *ex-situ* method to find the true $OH^-$ conductivity for AEMs by applying direct current and purging the carbonate species out of the membranes. We measured the true $OH^-$ conductivities and study the dynamics of the de-carbonation process of several commercially available and research AEMs. The true $OH^-$ conductivities values obtained using this novel method were found to be higher than the $OH^-$ conductivities reported in the literature using standard methods for the same membranes. This is since this conductivity measurement technique assures the AEMs are in their full $OH^-$ form, allowing to measure higher and correct $OH^-$ conductivities. The de-carbonation process was investigated at 40 °C and 95% RH for each of the AEMs. The time constant of the de-carbonation process was measured and found to be strongly affected by the IEC of the membrane, the current density used in the measurement, and the anion diffusivity coefficients. The time constant of the de-carbonation process decreases as the membrane IEC decreases and as the current density increases. Nevertheless, the shortest de-carbonation time was achieved for the lower ratio between $OH^-/HCO_3^-$ diffusivities, showing that the mobility of both ions is crucial for the $CO_2$ purging process in the AEM. This work provides distinctive and important data on the AEM de-carbonation process, crucial for the future understanding of the de-carbonation process for AEMFCs operating with ambient air (containing $CO_2$).

## Declaration of competing interest

The authors declare that they have no known competing financial interests or personal relationships that could have appeared to influence the work reported in this paper.

## Acknowledgment

This work was partially funded by the Nancy & Stephan Grand Technion Energy Program (GTEP); by the European Union's Horizon 2020 research and innovation program [grant No. 721065]; by the Ministry of Science, Technology & Space of Israel through grant No. 3–12948; by the Israel Science Foundation (ISF) [grant No. 1481/17]; and by the Ministry of National Infrastructure, Energy and Water Resources of Israel [grant No. 3-13671]; by the European Regional Development Fund [grant No. ZW6-85036745]. The authors would also like to acknowledge the financial support of Planning & Budgeting Committee/ISRAEL Council for Higher Education (CHE) and Fuel Choice Initiative (Prime Minister Office of Israel), within the framework of "Israel National Research Center for Electrochemical Propulsion (INREP) ". This research was also partially carried out within the United States-Israel Binational Science Foundation (BSF) [grant No. 2018171]. Finally, the authors would like to thank Prof. John Varcoe (Surrey University), Dr. Bryan Pivovar (National Renewable Energy Laboratory), Prof. Patric Jannasch (Lund University), Dr. Michael Schuster (Fumatech), and Prof. Kenji Miyatake (Yamanashi University) for their generous supply of the membrane samples used in this study.

## References

[1] N. Ralbag, M. Mann-Lahav, E.S. Davydova, U. Ash, R. Galed, M. Handl, R. Hiesgen, E. Magliocca, W. Mustain, J. He, P. Cong, A.M. Beale, G.S. Grader, D. Avnir, D. R. Dekel, Composite materials with combined electronic and ionic properties, Matter 1 (2019) 959–975, https://doi.org/10.1016/j.matt.2019.04.007.

[2] M. Bellini, M.V. Pagliaro, A. Lenarda, P. Fornasiero, M. Marelli, C. Evangelisti, M. Innocenti, Q. Jia, S. Mukerjee, J. Jankovic, L. Wang, J.R. Varcoe, C. B. Krishnamurthy, I. Grinberg, E. Davydova, D.R. Dekel, H.A. Miller, F. Vizza, Palladium–Ceria catalysts with enhanced alkaline hydrogen oxidation activity for anion exchange membrane fuel cells, ACS Appl. Energy Mater. 2 (2019) 4999–5008, https://doi.org/10.1021/acsaem.9b00657.

[3] H. Yu, E.S. Davydova, U. Ash, H.A. Miller, L. Bonville, D.R. Dekel, R. Maric, Palladium-ceria nanocatalyst for hydrogen oxidation in alkaline media: optimization of the Pd–CeO2 interface, Nanomater. Energy 57 (2019) 820–826, https://doi.org/10.1016/j.nanoen.2018.12.098.

[4] J.R. Varcoe, P. Atanassov, D.R. Dekel, A.M. Herring, M.a. Hickner, P.a. Kohl, A. R. Kucernak, W.E. Mustain, K. Nijmeijer, K. Scott, T. Xu, L. Zhuang, Anion-exchange membranes in electrochemical energy systems, Energy Environ. Sci. 7 (2014) 3135–3191, https://doi.org/10.1039/b000000x.

[5] D.R. Dekel, Alkaline membrane fuel cell (AMFC) materials and system improvement - state-of-the-art, ECS Trans 50 (2013) 2051–2052, https://doi.org/10.1149/05002.2051ecst.

[6] T.J. Omasta, L. Wang, X. Peng, C.A. Lewis, J.R. Varcoe, W.E. Mustain, Importance of balancing membrane and electrode water in anion exchange membrane fuel cells, J. Power Sources 375 (2018) 205–213, https://doi.org/10.1016/j.jpowsour.2017.05.006.

[7] L. Wang, X. Peng, W.E. Mustain, J.R. Varcoe, Radiation-grafted anion-exchange membranes: the switch from low- to high-density polyethylene leads to remarkably enhanced fuel cell performance, Energy Environ. Sci. 12 (2019) 1575–1579, https://doi.org/10.1039/C9EE00331B.

[8] T.J. Omasta, X. Peng, H.A. Miller, F. Vizza, L. Wang, J.R. Varcoe, D.R. Dekel, W. E. Mustain, Beyond 1.0 W cm $^2$ performance without platinum: the beginning of a

new era in anion exchange membrane fuel cells, J. Electrochem. Soc. 165 (2018) J3039–J3044, https://doi.org/10.1149/2.0071815jes.
[9] G. Huang, M. Mandal, X. Peng, A.C. Yang-neyerlin, B.S. Pivovar, W.E. Mustain, P. A. Kohl, Composite poly ( norbornene) anion conducting membranes for achieving durability , water management and high power (3 . 4 W/cm 2) in hydrogen/oxygen alkaline, Fuel Cell. 166 (2019) 637–644, https://doi.org/10.1149/2.1301910jes.
[10] D.R. Dekel, M. Amar, S. Willdorf, M. Kosa, S. Dhara, C.E. Diesendruck, Effect of water on the stability of quaternary ammonium groups for anion exchange membrane fuel cell applications, Chem. Mater. 29 (2017) 4425–4431, https://doi.org/10.1021/acs.chemmater.7b00958.
[11] D.R. Dekel, S. Willdorf, U. Ash, M. Amar, S. Pusara, S. Dhara, S. Srebnik, C. E. Diesendruck, The critical relation between chemical stability of cations and water in anion exchange membrane fuel cells environment, J. Power Sources 375 (2018) 351–360, https://doi.org/10.1016/j.jpowsour.2017.08.026.
[12] J. Fan, S. Willdorf-Cohen, E.M. Schibli, Z. Paula, W. Li, T.J.G. Skalski, A. T. Sergeenko, A. Hohenadel, B.J. Frisken, E. Magliocca, W.E. Mustain, C. E. Diesendruck, D.R. Dekel, S. Holdcroft, Poly(bis-arylimidazoliums) possessing high hydroxide ion exchange capacity and high alkaline stability, Nat. Commun. 10 (2019) 2306, https://doi.org/10.1038/s41467-019-10292-z.
[13] M.G. Marino, K.D. Kreuer, Alkaline stability of quaternary ammonium cations for alkaline fuel cell membranes and ionic liquids, ChemSusChem 8 (2015) 513–523, https://doi.org/10.1002/cssc.201403022.
[14] T. Huang, G. He, J. Xue, O. Otoo, X. He, H. Jiang, J. Zhang, Y. Yin, Z. Jiang, J. C. Douglin, D.R. Dekel, D. Michael, Self-crosslinked blend alkaline anion exchange membranes with bi-continuous phase separated morphology to enhance ion conductivity, J. Membr. Sci. (2020), https://doi.org/10.1016/j.memsci.2019.117769.
[15] K. Yassin, I.G. Rasin, S. Brandon, D.R. Dekel, Quantifying the critical effect of water diffusivity in anion exchange membranes for fuel cell applications, J. Membr. Sci. 608 (2020) 118206, https://doi.org/10.1016/j.memsci.2020.118206.
[16] G. Merle, M. Wessling, K. Nijmeijer, Anion exchange membranes for alkaline fuel cells: a review, J. Membr. Sci. 377 (2011) 1–35, https://doi.org/10.1016/j.memsci.2011.04.043.
[17] E.S. Davydova, S. Mukerjee, F. Jaouen, D.R. Dekel, Electrocatalysts for hydrogen oxidation reaction in alkaline electrolytes, ACS Catal. 8 (2018) 6665–6690, https://doi.org/10.1021/acscatal.8b00689.
[18] H.A. Miller, F. Vizza, M. Marelli, A. Zadick, L. Dubau, M. Chatenet, S. Geiger, S. Cherevko, H. Doan, R.K. Pavlicek, S. Mukerjee, D.R. Dekel, Highly active nanostructured palladium-ceria electrocatalysts for the hydrogen oxidation reaction in alkaline medium, Nanomater. Energy 33 (2017) 293–305, https://doi.org/10.1016/j.nanoen.2017.01.051.
[19] H.A. Miller, A. Lavacchi, F. Vizza, M. Marelli, F. Di Benedetto, F. D'Acapito, Y. Paska, M. Page, D.R. Dekel, A Pd/C-CeO2 anode catalyst for high-performance platinum-free anion exchange membrane fuel cells, Angew Chem. Int. Ed. Engl. 55 (2016), https://doi.org/10.1002/anie.201600647, 6004–7.
[20] D.R. Dekel, Unraveling mysteries of hydrogen electrooxidation in anion exchange membrane fuel cells, Curr. Opin. Electrochem. 12 (2018) 182–188, https://doi.org/10.1016/j.coelec.2018.11.013.
[21] N. Ziv, W.E. Mustain, D.R. Dekel, The effect of ambient carbon dioxide on anion-exchange membrane fuel cells, ChemSusChem 11 (2018) 1136–1150, https://doi.org/10.1002/cssc.201702330.
[22] N. Ziv, A.N. Mondal, T. Weissbach, S. Holdcroft, D.R. Dekel, Effect of CO2 on the properties of anion exchange membranes for fuel cell applications, J. Membr. Sci. 586 (2019) 140–150, https://doi.org/10.1016/j.memsci.2019.05.053.
[23] J. Peng, A.L. Roy, S.G. Greenbaum, T.A. Zawodzinski, Effect of CO2 absorption on ion and water mobility in an anion exchange membrane, J. Power Sources 380 (2018) 64–75, https://doi.org/10.1016/j.jpowsour.2018.01.071.
[24] Q. Duan, S. Ge, C.-Y. Wang, Water uptake, ionic conductivity and swelling properties of anion-exchange membrane, J. Power Sources 243 (2013) 773–778, https://doi.org/10.1016/j.jpowsour.2013.06.095.
[25] T.P. Pandey, A.M. Maes, H.N. Sarode, B.D. Peters, S. Lavina, K. Vezzù, Y. Yang, S. D. Poynton, J.R. Varcoe, S. Seifert, M.W. Liberatore, V. Di Noto, A.M. Herring, Interplay between water uptake, ion interactions, and conductivity in an e-beam grafted poly(ethylene-co-tetrafluoroethylene) anion exchange membrane, Phys. Chem. Chem. Phys. 17 (2015) 4367–4378, https://doi.org/10.1039/c4cp05755d.
[26] N. Ziv, D.R. Dekel, A practical method for measuring the true hydroxide conductivity of anion exchange membranes, Electrochem. Commun. 88 (2018) 109–113, https://doi.org/10.1016/j.elecom.2018.01.021.
[27] X. Cao, D. Novitski, S. Holdcroft, Visualization of hydroxide ion formation upon electrolytic water splitting in an anion exchange membrane, ACS Mater. Lett. 1 (2019) 362–366, https://doi.org/10.1021/acsmaterialslett.9b00195.
[28] J. Yan, M.A. Hickner, Anion exchange membranes by bromination of benzylmethyl-containing poly(sulfone)s, Macromolecules 43 (2010) 2349–2356, https://doi.org/10.1021/ma902430y.
[29] K.N. Grew, X. Ren, D. Chu, Effects of temperature and carbon dioxide on anion exchange membrane, Conductivity 14 (2011) 127–131, https://doi.org/10.1149/2.011112esl.
[30] E.R. Nightingale, Phenomenological theory of ion solvation. Effective radii of hydrated ions, J. Phys. Chem. 63 (1959) 1381–1387, https://doi.org/10.1021/j150579a011.
[31] B.W. Connors, B.R. Ransom, Chloride conductance and extracellular potassium concentration interact to modify the excitability of rat optic nerve fibres, J. Physiol. 355 (1984) 619–633, https://doi.org/10.1113/jphysiol.1984.sp015442.
[32] M. Piana, M. Boccia, A. Filpi, E. Flammia, H.A. Miller, M. Orsini, F. Salusti, S. Santiccioli, F. Ciardelli, A. Pucci, H2/air alkaline membrane fuel cell performance and durability, using novel ionomer and non-platinum group metal cathode catalyst, J. Power Sources 195 (2010) 5875–5881, https://doi.org/10.1016/j.jpowsour.2009.12.085.
[33] S. Gottesfeld, D.R. Dekel, M. Page, C. Bae, Y. Yan, P. Zelenay, Y.S. Kim, Anion exchange membrane fuel cells: current status and remaining challenges, J. Power Sources 375 (2018) 170–184, https://doi.org/10.1016/j.jpowsour.2017.08.010.
[34] A.G. Divekar, A.M. Park, Z.R. Owczarczyk, S. Seifert, B.S. Pivovar, A.M. Herring, A study of carbonate formation kinetics and morphological effects observed on OH - form of pfaem when exposed to air containing CO 2, ECS Trans 80 (2017) 1005–1011, https://doi.org/10.1149/08008.1005ecst.
[35] H. Yanagi, K. Fukuta, Anion exchange membrane and ionomer for alkaline membrane fuel cells (AMFCs), in: ECS Trans, ECS, 2008, pp. 257–262, https://doi.org/10.1149/1.2981860.
[36] S. Suzuki, H. Muroyama, T. Matsui, K. Eguchi, Influence of CO2 dissolution into anion exchange membrane on fuel cell performance, Electrochim. Acta 88 (2013) 552–558, https://doi.org/10.1016/j.electacta.2012.10.105.
[37] Y. Zheng, T.J. Omasta, X. Peng, L. Wang, J.R. Varcoe, B.S. Pivovar, W.E. Mustain, Quantifying and elucidating the effect of CO 2 on the thermodynamics, kinetics and charge transport of AEMFCs, Energy Environ. Sci. 12 (2019) 2806–2819, https://doi.org/10.1039/C9EE01334B.
[38] J. Xue, X. Liu, J. Zhang, Y. Yin, M.D. Guiver, Poly(phenylene oxide)s incorporating N-spirocyclic quaternary ammonium cation/cation strings for anion exchange membranes, J. Membr. Sci. (2019) 117507, https://doi.org/10.1016/j.memsci.2019.117507.
[39] a.M. Kiss, T.D. Myles, K.N. Grew, a. a. Peracchio, G.J. Nelson, W.K.S. Chiu, Carbonate and bicarbonate ion transport in alkaline anion exchange membranes, J. Electrochem. Soc. 160 (2013) F994–F999, https://doi.org/10.1149/2.037309jes.
[40] K.N. Grew, D. Chu, W.K.S. Chiu, Ionic equilibrium and transport in the alkaline anion exchange membrane, J. Electrochem. Soc. 157 (2010) B1024, https://doi.org/10.1149/1.3368728.
[41] A. Amel, N. Gavish, L. Zhu, D.R. Dekel, M.A. Hickner, Y. Ein-Eli, Bicarbonate and chloride anion transport in anion exchange membranes, J. Membr. Sci. 514 (2016) 125–134, https://doi.org/10.1016/j.memsci.2016.04.027.
[42] K.N. Grew, W.K.S. Chiu, A dusty fluid model for predicting hydroxyl anion conductivity in alkaline anion exchange membranes, J. Electrochem. Soc. 157 (2010) B327, https://doi.org/10.1149/1.3273200.
[43] M.E. Tuckerman, D. Marx, M. Parrinello, The Nature and Transport Mechanism of Hydrated Hydroxide Ions in Aqueous Solution, vol. 417, 2002, pp. 925–929, https://doi.org/10.1038/nature00794.1.
[44] J.A. Vega, C. Chartier, W.E. Mustain, Effect of hydroxide and carbonate alkaline media on anion exchange membranes, J. Power Sources 195 (2010) 7176–7180, https://doi.org/10.1016/j.jpowsour.2010.05.030.
[45] S. Srebnik, S. Pusara, D.R. Dekel, Effect of carbonate anions on quaternary ammonium-hydroxide interaction, J. Phys. Chem. C 123 (2019) 15956–15962, https://doi.org/10.1021/acs.jpcc.9b03131.
[46] K. Fukuta, H. Inoue, S. Watanabe, H. Yanagi, In-situ observation of CO2 through the self-purging in alkaline membrane fuel cell (AMFC), in: ECS Trans, 2009, pp. 23–27, https://doi.org/10.1149/1.3271358.
[47] S. Watanabe, K. Fukuta, H. Yanagi, Determination of Carbonate Ion in MEA during the Alkaline Membrane Fuel Cell, (AMFC) Operation, 2010, pp. 1837–1845, https://doi.org/10.1149/1.3484674.
[48] L. Wang, X. Peng, W.E. Mustain, J.R. Varcoe, Radiation-grafted anion-exchange membranes: the switch from low- to high-density polyethylene leads to remarkably enhanced fuel cell performance, Energy Environ. Sci. 12 (2019) 1575–1579, https://doi.org/10.1039/c9ee00331b.
[49] J. Müller, A. Zhegur, U. Krewer, J.R. Varcoe, D.R. Dekel, Practical ex-situ technique to measure the chemical stability of anion-exchange membranes under conditions simulating the fuel cell environment, ACS Mater. Lett. 2 (2020) 168–173, https://doi.org/10.1021/acsmaterialslett.9b00418.
[50] J. Ponce-González, D.K. Whelligan, L. Wang, R. Bance-Soualhi, Y. Wang, Y. Peng, H. Peng, D.C. Apperley, H.N. Sarode, T.P. Pandey, A.G. Divekar, S. Seifert, A. M. Herring, L. Zhuang, J.R. Varcoe, High performance aliphatic-heterocyclic benzyl-quaternary ammonium radiation-grafted anion-exchange membranes, Energy Environ. Sci. 9 (2016) 3724–3735, https://doi.org/10.1039/C6EE01958G.
[51] L. Wang, M. Bellini, H.A. Miller, J.R. Varcoe, A high conductivity ultrathin anion-exchange membrane with 500+ h alkali stability for use in alkaline membrane fuel cells that can achieve 2 W cm-2 at 80 °c, J. Mater. Chem. A. 6 (2018) 15404–15412, https://doi.org/10.1039/c8ta04783a.
[52] A.M. Park, Z.R. Owczarczyk, L.E. Garner, A.C. Yang-Neyerlin, H. Long, C. M. Antunes, M.R. Sturgeon, M.J. Lindell, S.J. Hamrock, M. Yandrasits, B.S. Pivovar, Synthesis and characterization of perfluorinated anion exchange membranes, ECS Trans 80 (2017) 957–966, https://doi.org/10.1149/08008.0957ecst.
[53] J.S. Olsson, T.H. Pham, P. Jannasch, Tuning poly(arylene piperidinium) anion-exchange membranes by copolymerization, partial quaternization and crosslinking, J. Membr. Sci. 578 (2019) 183–195, https://doi.org/10.1016/j.memsci.2019.01.036.
[54] H. Ono, T. Kimura, A. Takano, K. Asazawa, J. Miyake, J. Inukai, K. Miyatake, Robust anion conductive polymers containing perfluoroalkylene and pendant ammonium groups for high performance fuel cells, J. Mater. Chem. A. 5 (2017) 24804–24812, https://doi.org/10.1039/c7ta09409d.
[55] Y. Zheng, U. Ash, R.P. Pandey, A.G. Ozioko, J. Ponce-González, M. Handl, T. Weissbach, J.R. Varcoe, S. Holdcroft, M.W. Liberatore, R. Hiesgen, D.R. Dekel, Water uptake study of anion exchange membranes, Macromolecules 51 (2018) 3264–3278, https://doi.org/10.1021/acs.macromol.8b00034.

[56] K. Xu, M.A. Hickner, C.S. Ewing, Q. Wang, P.M. Mangiagli, Dynamic water uptake of flexible ion-containing polymer networks, Fuel Cell. 9 (2009) 432–438, https://doi.org/10.1002/fuce.200800157.
[57] J. Peng, A.L. Roy, S.G. Greenbaum, T.A. Zawodzinski, Effect of CO2 absorption on ion and water mobility in an anion exchange membrane, J. Power Sources 380 (2018) 64–75, https://doi.org/10.1016/j.jpowsour.2018.01.071.
[58] L. Wang, J.J. Brink, Y. Liu, A.M. Herring, J. Ponce-González, D.K. Whelligan, J. R. Varcoe, Non-fluorinated pre-irradiation-grafted (peroxidated) LDPE-based anion-exchange membranes with high performance and stability, Energy Environ. Sci. 10 (2017) 2154–2167, https://doi.org/10.1039/c7ee02053h.
[59] Z. Liu, X. Li, K. Shen, P. Feng, Y. Zhang, X. Xu, W. Hu, Z. Jiang, B. Liu, M.D. Guiver, Naphthalene-based poly(arylene ether ketone) anion exchange membranes, J. Mater. Chem. A. 1 (2013) 6481, https://doi.org/10.1039/c3ta10355b.
[60] A. Ouadah, H. Xu, T. Luo, S. Gao, Z. Zhang, Z. Li, C. Zhu, Synthesis of novel copolymers based on: P -methylstyrene, N, N -butylvinylimidazolium and polybenzimidazole as highly conductive anion exchange membranes for fuel cell application, RSC Adv. 7 (2017) 47806–47817, https://doi.org/10.1039/c7ra06394f.
[61] C. Lu, C. Long, Y. Li, Z. Li, H. Zhu, Chemically stable poly(meta-terphenyl piperidinium) with highly conductive side chain for alkaline fuel cell membranes, J. Membr. Sci. (2020) 117797, https://doi.org/10.1016/j.memsci.2019.117797.
[62] B. Shi, J. Zhang, W. Wu, J. Wang, J. Huang, Controlling conduction environments of anion exchange membrane by functionalized SiO2 for enhanced hydroxide conductivity, J. Membr. Sci. 569 (2019) 166–176, https://doi.org/10.1016/j.memsci.2018.10.020.
[63] J. Li, B. Zhang, H. Wu, L. Cao, X. He, Y. Li, M. Xu, Z. Jiang, Incorporating imidazolium-functionalized graphene oxide into imidazolium-functionalized poly (ether ether ketone) for enhanced hydroxide conductivity, J. Membr. Sci. 565 (2018) 233–240, https://doi.org/10.1016/j.memsci.2018.08.022.
[64] M. Qiu, B. Zhang, H. Wu, L. Cao, X. He, Y. Li, J. Li, M. Xu, Z. Jiang, Preparation of anion exchange membrane with enhanced conductivity and alkaline stability by incorporating ionic liquid modified carbon nanotubes, J. Membr. Sci. 573 (2019) 1–10, https://doi.org/10.1016/j.memsci.2018.11.070.
[65] X. Ge, Y. He, M.D. Guiver, L. Wu, J. Ran, Z. Yang, T. Xu, Alkaline anion-exchange membranes containing mobile ion shuttles, Adv. Mater. 28 (2016) 3467–3472, https://doi.org/10.1002/adma.201506199.
[66] Z. Yang, R. Guo, R. Malpass-Evans, M. Carta, N.B. McKeown, M.D. Guiver, L. Wu, T. Xu, Highly conductive anion-exchange membranes from microporous troger's base polymers, Angew. Chem. 128 (2016) 11671–11674, https://doi.org/10.1002/ange.201605916.
[67] A.M. Ahmed Mahmoud, A.M. Mohamed Elsaghier, K. Miyatake, Effect of ammonium groups on the properties of anion conductive membranes based on partially fluorinated aromatic polymers, RSC Adv. 6 (2016) 27862–27870, https://doi.org/10.1039/C6RA03256G.
[68] H. Zarrin, G. Jiang, G.Y.Y. Lam, M. Fowler, Z. Chen, High performance porous polybenzimidazole membrane for alkaline fuel cells, Int. J. Hydrogen Energy 39 (2014) 18405–18415, https://doi.org/10.1016/j.ijhydene.2014.08.134.
[69] I. Masel Richard, Anion exchange membrane electrolyzers with base metal catalysts showing 1 A/cm2 at 1.75 V. http://www.ice2017.net/-/media/Sites/Ice2017/Uploads/ICE2017_027_Masel.ashx?la da&hash 2295401BFD54C8B679B95F78105BBCE135DA8D8E, 2017.
[70] H. Peng, Q. Li, M. Hu, L. Xiao, J. Lu, L. Zhuang, Alkaline polymer electrolyte fuel cells stably working at 80 °C, J. Power Sources 390 (2018) 165–167, https://doi.org/10.1016/j.jpowsour.2018.04.047.
[71] A.G. Divekar, M. Kuo, A.M. Park, A.R. Motz, Z.S. Page-Belknap, Z. Owczarczyk, H. Long, S. Seifert, C.M. Maupin, M.A. Yandrasits, Y. Yang, B.S. Pivovar, A. M. Herring, The impact of alkyl tri-methyl ammonium side chains on perfluorinated ionic membranes for electrochemical applications, J. Polym. Sci., Part B: Polym. Phys. 57 (2019) 700–712, https://doi.org/10.1002/polb.24825.
[72] T. Zelovich, L. Vogt-Maranto, M.A. Hickner, S.J. Paddison, C. Bae, D.R. Dekel, M. E. Tuckerman, Hydroxide ion diffusion in anion-exchange membranes at low hydration: insights from ab initio molecular dynamics, Chem. Mater. 31 (2019) 5778–5787, https://doi.org/10.1021/acs.chemmater.9b01824.
[73] M.G. Marino, J.P. Melchior, A. Wohlfarth, K.D. Kreuer, Hydroxide, halide and water transport in a model anion exchange membrane, J. Membr. Sci. 464 (2014) 61–71, https://doi.org/10.1016/j.memsci.2014.04.003.
[74] I. Zadok, D.R. Dekel, S. Srebnik, Effect of ammonium cations on the diffusivity and structure of hydroxide ions in low hydration media, J. Phys. Chem. C 123 (2019) 27355–27362, https://doi.org/10.1021/acs.jpcc.9b07881.
[75] T. Zelovich, Z. Long, M. Hickner, S.J. Paddison, C. Bae, M.E. Tuckerman, Ab initio molecular dynamics study of hydroxide diffusion mechanisms in nanoconfined structural mimics of anion exchange membranes, J. Phys. Chem. C 123 (2019) 4638–4653, https://doi.org/10.1021/acs.jpcc.8b10298.
[76] T. Zelovich, M.E. Tuckerman, Water layering affects hydroxide diffusion in functionalized nanoconfined environments, J. Phys. Chem. Lett. (2020) 5087–5091, https://doi.org/10.1021/acs.jpclett.0c01141.
[77] I. Zadok, H. Long, B. Pivovar, A. Roznowska, A. Michalak, D.R. Dekel, S. Srebnik, Unexpected hydroxide ion structure and properties at low hydration, J. Mol. Liq. 313 (2020) 113485, https://doi.org/10.1016/j.molliq.2020.113485.
[78] I. Nicotera, V. Kosma, C. Simari, G.A. Ranieri, M. Sgambetterra, S. Panero, M. A. Navarra, An NMR study on the molecular dynamic and exchange effects in composite Nafion/sulfated titania membranes for PEMFCs, Int. J. Hydrogen Energy 40 (2015) 14651–14660, https://doi.org/10.1016/j.ijhydene.2015.06.137.
[79] D. Dong, W. Zhang, A. Barnett, J. Lu, A. van Duin, V. Molinero, D. Bedrov, Multiscale modeling of structure, transport and reactivity in alkaline fuel cell membranes: combined coarse-grained, atomistic and reactive molecular dynamics simulations, Polymers 10 (2018) 1289, https://doi.org/10.3390/polym10111289.
[80] A. Jasti, S. Prakash, V.K. Shahi, Stable and hydroxide ion conductive membranes for fuel cell applications: chloromethyaltion and amination of poly(ether ether ketone), J. Membr. Sci. 428 (2013) 470–479, https://doi.org/10.1016/j.memsci.2012.11.016.
[81] N. Li, M.D. Guiver, W.H. Binder, Towards high conductivity in anion-exchange membranes for alkaline fuel cells, ChemSusChem 6 (2013) 1376–1383, https://doi.org/10.1002/cssc.201300320.
[82] A. Zhegur, N. Gjineci, S. Willdorf-Cohen, A.N. Mondal, C.E. Diesendruck, N. Gavish, D.R. Dekel, Changes of anion exchange membrane properties during chemical degradation, ACS Appl. Polym. Mater. 2 (2020) 360–367, https://doi.org/10.1021/acsapm.9b00838.